Control of the ferroelectric properties of DyMn$_2$O$_5$ by magnetic fields

D. Higashiyama and S. Miyasaka

Department of Applied Physics, University of Tokyo, Tokyo 113-8656, Japan

N. Kida

Spin Superstructure Project (SSS), ERATO, Japan Science and Technology Agency (JST),
c/o National Institute of Advanced Industrial Science and Technology, Tsukuba 305-8562, Japan

T. Arima

Institute of Materials Science, University of Tsukuba, Tsukuba 305-8573, Japan
and Spin Superstructure Project (SSS), ERATO, Japan Science and Technology Agency (JST),
c/o National Institute of Advanced Industrial Science and Technology, Tsukuba, 305-8562, Japan

Y. Tokura

Department of Applied Physics, University of Tokyo, Tokyo 113-8656, Japan;
Spin Superstructure Project (SSS), ERATO, Japan Science and Technology Agency (JST), c/o National Institute of Advanced Industrial
Science and Technology, Tsukuba 305-8562, Japan;
and Correlated Electron Research Center (CERC), National Institute of Advanced Industrial Science and Technology (AIST),
Tsukuba 305-8562, Japan

Coupling between magnetic and dielectric properties has been attracting renewed interest because of the fundamental as well as technological importance of controlling the electric (magnetic) polarization by an external magnetic (electric) field. Here, we report the phenomenon that an external magnetic field induces and/or modifies ferroelectric states in a magnetic material, DyMn$_2$O$_5$. Measurements of the temperature dependence of hysteretic polarization curves, pyroelectric current, specific heat, optical second harmonic generation, and x-ray superlattice peaks have revealed successive phase transitions between 43 and 4 K, accompanying three ferroelectric phases. The zero-field lowest-temperature phase (<8 K) induced by the Dy-moment ordering is a reentrant paraelectric state, but is turned into a ferroelectric state with increasing magnetic field. The phenomenon is closely related to the metamagnetic transitions of the Dy f moment, indicating that all the ferroelectric phases of this material are strongly tied to the antiferromagnetic Mn spin structure affected by the f-d exchange interaction. The electric phase diagram for DyMn$_2$O$_5$ is presented in the plane of temperature and magnetic field.

I. INTRODUCTION

Controlling the electric polarization by a magnetic field, or inversely the magnetization by an electric field has long been an important and interesting topic, and is commonly known as the magneto-electric (ME) effect. This possibility was first predicted by Pierre Curie[1] in 1894, but its reality in a substantial material Cr$_2$O$_3$ was pointed out by Dzyaloshinskiĭ[2] in 1959 and experimentally demonstrated by Astrov[3] in 1960. Since then, the ME effect has been observed in many materials.[4–6] Studies of the ME effect have been providing fundamentally important information about the cross correlation between the magnetic and electric polarizations, yet its magnitude has remained too small for actual technological application of this intriguing phenomenon to be realized. A key to the breakthrough is believed to be the use of *multiferroics*, materials in which (anti)ferromagnetic and (anti)ferroelectric order coexist.

Although materials that are simultaneously ferromagnetic and ferroelectric are quite rare, several families of magnetic ferroelectrics have been reported in which the spontaneous electric polarization can be controlled to a considerable extent by an external magnetic field. The first example is weakly ferromagnetic boracite Ni$_3$B$_7$O$_{13}$I as reported by Schmid and co-workers,[7] in which the rotation of the magnetic field by 90° causes a 180° switching of the spontaneous electric polarization. Quite recently, Kimura *et al.*[8] have demonstrated an approach to the magnetic field control of the spontaneous polarization. In the orthorhombically distorted perovskite TbMnO$_3$, the ferroelectric polarization emerges from the incommensurate (IC) to commensurate (C) antiferromagnetic transition. Below 10 K, the Tb 4f moments order is due to a coupling with the Mn d-electron spins. Here, a magnetic field can induce a metamagnetic transition related to the flop of the Tb moments, perhaps altering the commensurate Mn spin structure, and produce a 90° flop of the spontaneous polarization. The key ingredients needed for such magnetic field effects are: (1) a commensurate d-electron spin structure that couples magneto elastically with the lattice modulation producing the spontaneous polarization, and (2) an f-d exchange interaction that amplifies the action of the external magnetic field to alter the d-electron spin state. In this context, a similar mechanism for magnetic field control may apply to other rare-earth transition-metal oxides that show magnetic-order induced ferroelectricity. Apart from the family of RMnO$_3$ perovskites (R=Gd,Tb,Dy),[9] one such
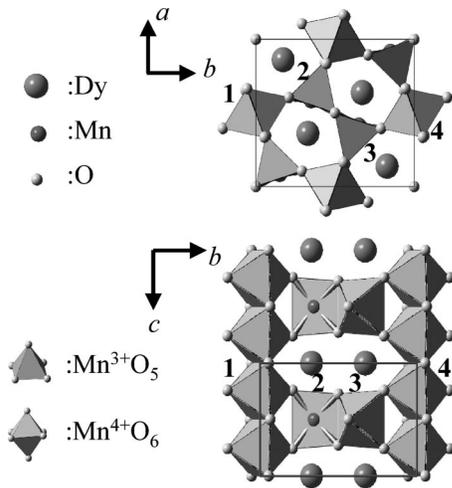
FIG. 1. Crystal structure of $DyMn_2O_5$: A view along the *c* axis (upper panel) and along the *a* axis for the sub cells labeled 1, 2, 3 and 4 (lower panel).

promising candidate material is RMn_2O_5 (R=a rare earth ion, Y, or Bi), which exhibits with magnetically induced ferroelectricity.[10] Here, we report the variation of the ferroelectric phases with application of an external magnetic field in $DyMn_2O_5$. The most striking feature found in this study is that the ferroelectric states are successively induced in the paraelectric ground state by applying a magnetic field. This may be viewed as a type of gigantic ME effect. We present here the electric phase diagram in the plane of temperature and magnetic field for $DyMn_2O_5$.

The RMn_2O_5 compounds are magnetic ferroelectrics that undergo a ferroelectric transition at $25-39$ K below an antiferromagnetic transition temperature $T_N=39-45$ K.[10] According to structural studies,[11,12] the orthorhombic crystal ($Pbam$) at room temperature is composed of $Mn^{4+}O_6$ octahedral and $Mn^{3+}O_5$ pyramidal units as shown in Fig. 1. The octahedra form chains along the *c* axis while sharing their edges. On the other hand, a pair of pyramids links these chains within the *ab* plane. The emergence of ferroelectricity is believed to arise from the pyramidal Mn^{3+} sites.[13] The magnetic structure of $DyMn_2O_5$ was determined using neutron diffraction by Wilkinson *et al.*[14] At 4.2 K the antiferromagnetic state is characterized by the two magnetic propagation vectors $(1/2\ 0\ 0)$ and $[(1+\delta)/2\ 0\ 1/4]$ with $\delta \sim 0.001$. The Mn^{4+} octahedra form ferromagnetic chains with a spin moment of 2.0 μ_B, while the Mn^{4+} spin component perpendicular to the ferromagnetic component is antiferromagnetically modulated with an amplitude of 2.6 μ_B and a periodicity of $4c$. With increasing temperature, it was observed[14] that the $(h/2\ k\ 0)$ magnetic superlattice peaks (and thus the ferromagnetic component in each Mn^{4+} chain) disappear at 8 K (perhaps corresponding to T_X that we define later), which should result from disordering of the Dy moments. The magnetic scattering corresponding to the $[(1+\delta)/2\ 0\ 1/4]$ modulation persists above 8 K. The $[(h\pm\delta)/2\ \ell\pm1/4]$ split peaks merge to $(h/2\ 0\ \ell\pm1/4)$ at 18 K($=T_3$), and finally these antiferromagnetic peaks disappear about 44 ± 2 K($=T_N$). $DyMn_2O_5$ undergoes such compli-

cated successive magnetic transitions with varying temperature, indicating that there are competing exchange interactions among the Mn spins as well as coupling between the Mn spins and Dy moments. Here, we fully resolve the interrelation of the ferroelectricity/paraelectricity with the respective spin-ordered phases by measurements of dielectric constant, spontaneous polarization, specific heat, and magnetic susceptibility.

II. EXPERIMENT

Single crystals of $DyMn_2O_5$ (several mm in size) were grown with use of $PbO-PbF_2$ flux.[15] The oriented samples of rectangular shape with well-developed crystal surfaces of (001), (010), and (100) were prepared with use of back-Laue photographs. For the measurement of *P-E* curves, the triangular wave electric field (*E*) of 10 Hz was applied on the sample capacitor. The dielectric constant was measured by a commercial *LCR* meter (HP4274A) operated at 1 kHz while cooling the sample at a rate of 5 K/min. The specific heat was measured by a relaxation method in the cooling run at a rate of $\sim$0.3 K/min. Concerning the derivation of the spontaneous polarization (P_s) from the pyroelectric measurement, special caution should be paid to the present material. This is because the lowest-temperature phase of $DyMn_2O_5$ is the zero-P_s state (see Sec. III) and accordingly the conventional procedure of the electric-field cooling and the subsequent zero-electric-field warming procedure for the pyroelectric current measurement is invalidated. Therefore, we have measured the pyroelectric current with use of an electrometer (KEITHLEY6517A) while applying a relatively small electric field (200 kV/m) in the cooling run. Also when the magnetic field was scanned at a rate of 38 Oe/s, the pyroelectric current was measured while applying the electric field. Therefore, the polarization value for the final state in the course of the temperature or magnetic-field scan may be slightly affected by a tiny leak current and give some uncertainty in the obtained value. Nevertheless, such an electric-field-applied measurement is indispensable for the case where the zero-polarization state is involved during the temperature and/or magnetic field scans as in $DyMn_2O_5$.

We have also adopted the second harmonic (SH) generation technique to confirm the breaking of centrosymmetry induced by the ferroelectric order. The *s*-polarized fundamental light (the electric field *E* being set parallel to the ferroelectric *b* axis) of 1 mW from a Ti:sapphire regenerative amplifier system (the center wavelength of 800 nm, the pulse width of 130 fs, and the repetition rate of 1 kHz) was irradiated on the *ab* surface with the focused spot diameter of 0.5 mm and the incidence angle of 40°. The generated *s*-polarized ($\|b$) SH light was detected by a photomultiplier tube attached to a monochromator and a boxcar averager. The sample was once cooled to 20 K at a rate of 2 K/min in a poling field of 1.5 MV/m. After the poling field is removed at 20 K, SH measurements were performed in the warming and cooling runs.

The superlattice structure associated with the ferroelectric order in the spin-ordered state was searched in the reciprocal space of ($h\ 0\ \ell$) in terms of synchrotron-radiation x-ray dif-
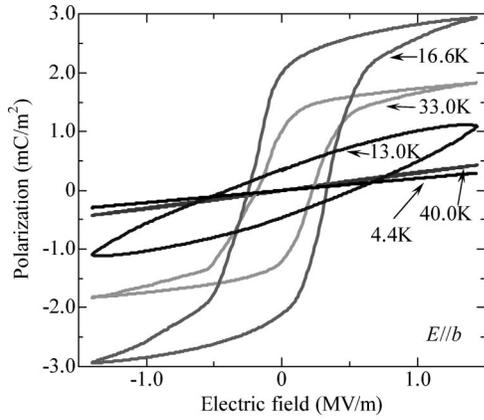
FIG. 2. The polarization (P) vs electric-field (E, 10 Hz) curves at various temperatures in the spin-ordered state of DyMn$_2$O$_5$. The ferroelectric states show the hysteretic P-E curves (at 33.0, 16.6, and 13.0 K in the figure), while the linear ones stand for the paraelectric states (at 40.0 and 4.4 K).

fraction. The measurements were performed by using a Huber six-axis diffractometer at Beam Line-4C, Photon Factory of KEK, Japan. The incident x-ray was monochromated at 13 keV by utilizing a Si (1 1 1) double-crystal monochromator and focused on a (001) surface of the single crystal mounted in a closed-cycle He refrigerator. To reduce the contamination of luminous x ray, a pyrographite (0 0 2) monochromator was installed in front of the scintillation counter.

III. RESULTS AND DISCUSSION

A. Ferroelectric and paraelectric states coupled with *d*-spin and *f*-moment orders

Let us first present unambiguous evidence for the ferroelectricity of DyMn$_2$O$_5$ crystal at low temperatures. Figure 2 exemplifies the P-E hysteretic curves at some selected temperatures in the cooling process. The electric field was applied along the b axis, since the spontaneous polarization (P_s), if any, is always observed along the b axis. Above 40 K, even below the magnetic ordering temperature ($T_N = 43$ K), the P-E curve is characteristic of paraelectrics, showing no P_s. As decreasing temperature below 40 K, the clear hysteresis loop characteristic of ferroelectrics is observed, and the remanent polarization as well as the coercive force is increased to reach the maximum around 26 K. The value of the P at zero E is plotted against temperature with closed circles in Fig. 3(d) to show the temperature variation of P_s. Below 13 K, however, the coercive force appears to steeply increase, and accordingly the P does not show the saturation even at 1.4 MV/m and the P-E curve shows a rounded shape as a whole. The obtained low P_s value at zero E [see also Fig. 3(d)] in this temperature range thus underestimates the real P_s that should be much larger, as discussed later in comparison with other P_s data derived by the pyroelectric current [Fig. 3(e)]. As a remarkable fact, the P-E curve below 7 K again shows no ferroelectric P-E curve. This indicates that the lowest-temperature phase below 7 K is a reentrant paraelectric state with no P_s. The *antiferroelec-*
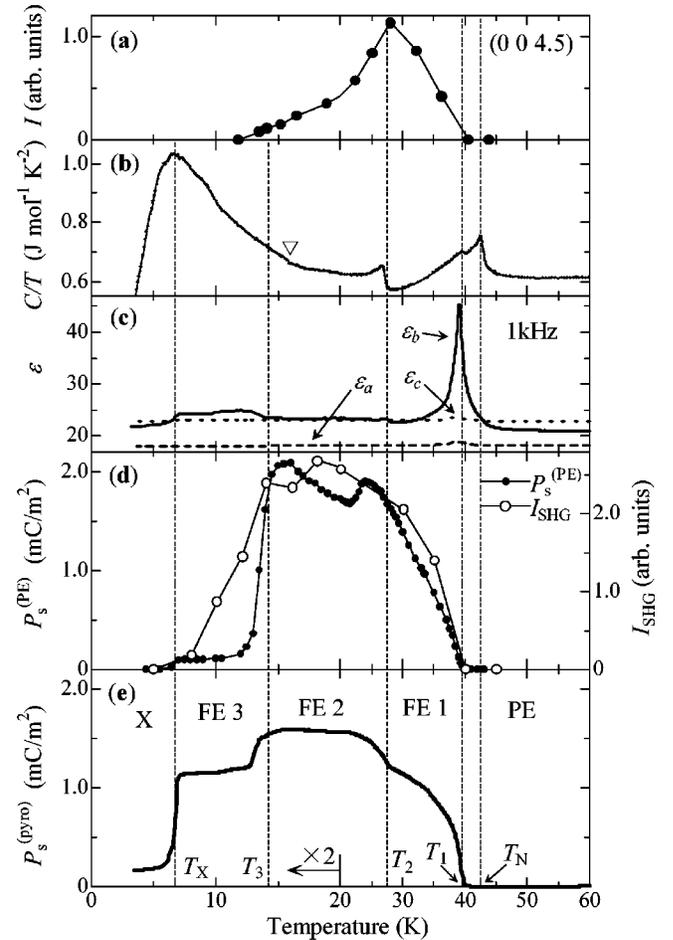

FIG. 3. The temperature dependence of several quantities related to the magnetic and/or dielectric phase transitions in DyMn$_2$O$_5$; (a) the integrated intensity (I) of x-ray superlattice peak at (0 0 4.5) shown in Fig. 4, (b) the specific heat (C) divided by temperature (T), (c) the dielectric constants for applied electric fields (1 kHz) along the a, b and c axis, (d) the spontaneous polarization ($P_s^{(PE)}$, closed circles) along the b axis obtained from the polarization vs electric-field (P-E) curves shown in Fig. 2, and (e) the polarization ($P_s^{(pyro)}$) along the b axis obtained by the measurement of pyroelectric current under an applied electric field of 200 kV/m. All the above temperature scans were done in the cooling run. In the panel (d), the temperature dependence of the second harmonic light intensity I_{SHG} is shown with open circles.

tric state might be possible, but the field-induced polarization cannot be observed up to 1.8 MV/m, above which the crystal shows dielectric breakdown. In accord with the emergence of the ferroelectric state, we have confirmed the SH generation of the b-polarized incident light. The SH light intensity, that is expected to be in proportion with square of P_s, was observed to decrease to the background level in the paraelectric phases at the temperatures below 7 K (down to 4.2 K) as well as above 40 K, as shown with open circles in Fig. 3(d). Here, we assumed the temperature-independent background signal above 40 K, perhaps arising from surface effects, as the zero level of the ferroelectricity-induced SH signal.

Figure 3 compares the temperature dependencies of (a) the x-ray superlattice peak observed at (0 0 4.5), (b) the

specific heat C divided by temperature T, (c) the dielectric constant ε measured with applied electric field (1 kHz) along the respective crystallographic axes, (d) P_s as deduced from the P-E curves (Fig. 2), and (e) P_s as deduced by the pyroelectric current during the electric-field (200 kV/m) cooling. (Note the change of the temperature scale on the abscissa below and above 20 K.) From these comprehensive measurements, we could reveal the five successive phase transitions occurring in DyMn$_2$O$_5$. First, the compound undergoes the antiferromagnetic transition, perhaps associated with the IC spin order, at T_N=43 K, and then the ferroelectric transition at T_1=40 K immediately below the T_N. These critical temperatures are close to each other but definitely distinguished as the double peaks in the specific heat data shown in Fig. 3(b). Around T_1, only the b-axis component of the dielectric constant shows a sharp anomaly as demonstrated in Fig. 3(c), in accord with the presence of the spontaneous polarization along the b axis in the lower-lying phases. (A tiny bump discerned in ε_a at T_1 is perhaps the leak component of the ε_b due to the slight misorientation of the sample.) The x-ray superlattice reflection at (0 0 4.5) is observed to increase in lowering temperature from T_1, but tends to decrease in intensity below 28 K ($=T_2$) and then finally disappears around 13 K ($=T_3$), as shown in Fig. 3(a) and Fig. 4. The emergence of such a C lattice modulation (see Fig. 4 for the observed peak profiles) is likely to correspond to the magnetic modulation with the propagation vector (1/2 0 1/4) reported in the temperature range between 18 and 44 K by Wilkinson *et al.*[14] When the spin exchange interaction is effective modulated by lattice dilation, such a spin-lattice coupling may give rise to the periodic lattice modulation with a half periodicity of the spin modulation. As observed in the case of the ferroelectric perovskite-type RMnO$_3$,[8] this type of exchange-striction effect inherent to the Mn-O network produces the lattice modulation with twice the modulation vector of the spin modulation. In analogy to the improper ferroelectrics like Rb$_2$ZnCl$_4$ and related compounds[16,17] as well as to perovskite RMnO$_3$, the IC to C transition of lattice modulation may also produce the parasitic ferroelectricity in this compound. What is unique in this system is the presence of multiple ferroelectric (FE1, FE2, and FE3) phases perhaps associated with the reordering of the spin state. All these ferroelectric phases show the spontaneous polarization only along the b axis.

The FE1-to-FE2 and FE2-to-FE3 transitions at $T_2 \sim 28$ K and $T_3 \sim 13$ K (on cooling), respectively, are clearly discerned as the sudden changes of P_s in Figs. 3(d) and 3(e). These transition temperatures are to some extent, up to ± 2 K, sample dependent, possibly due to slight oxygen off stoichiometry. The former transition is also manifested by the clear anomaly of the specific heat shown in Fig. 3(b). A tiny discontinuity of the specific heat around 16 K [indicated by an open triangle in Fig. 3(b)] may correspond to the FE2-to-FE3 transition. The phase transition between FE2 and FE3 shows a thermal hysteresis (a difference in the transition points in cooling and warming runs, $\Delta T_3 \sim 4$ K), indicating its first-order nature. The FE3 phase shows the large coercive force (>0.6 MV/m) as shown in Fig. 2, but the P_s estimated from the electric-field cooling pyroelectric current shows the

comparable value with other FE phases [see Fig. 3(e)]. The respective ferroelectric phases and their variation appear to be closely related to the successive emergence of the spin order with different propagation vectors (k_s). In fact, the lattice modulation caused by the commensurate [k_s=(1/2 0 1/4)] spin order can be seen as the superlattice peaks at $2k_s$ in the FE1 and FE2 phases. However, we could not observe (δ 0 9/2) superlattice in the FE3 phase [see the 11.8 K curve in Fig. 4(a)], which implies that the displacement of Mn and O atoms may change in direction and become confined within the ab plane. From the present combined measurements, the spin state transitions seem to be even more complex than reported in the literature,[14] which may miss the spin reorientation transitions corresponding to the PE($<T_N$)-FE1 and FE1-FE2 transitions at T_1 and T_2, respectively, and need to be carefully reexamined to correlate with the five ferroelectric/paraelectric phases below T_N.

With further lowering temperature, the compound undergoes the phase transition from the FE3 to the new paraelectric state, here referred to as the phase X, around T_X=7 K. This transition shows the thermal hysteresis ($\Delta T_X \sim 1$ K). The first-order nature of the transition is also evidenced by a steep drop of the P_s. The seemingly residual $P_s^{(\text{pyro})}$ in the phase X as seen in Fig. 3(e), as contrasted by zero $P_s^{(\text{PE})}$ in Fig. 3(d), might be due to the subsisting coexistence of the FE3 state due to the first-order nature of the transition, but more plausibly due to the leak current arising from the electric-field cooling measurement of the pyroelectric current. The conventional electric-field-cooling and zero-electric-field-warming procedure cannot be applied to the present material, since the lowest-temperature phase X shows no P_s, as described in Sec. II. This paraelectric phase X is obviously related to the ordering of the Dy f-electron moments (and resultant modification of d-electron spins) as manifested by the corresponding large peak in the specific heat [Fig. 3(b)]. Ordering of the Dy moments also affects the spin ordering of Mn^{3+} and Mn^{4+}, as revealed by Wilkinson *et al.*[14] Upon the f-moment ordering, the spin structure in a Mn^{4+} chain along the c axis changes from the purely antiferromagnetic state with a periodicity of $4c$ to the ferrimagnetic one. The exchange striction and parasitic ferroelectricity can result only from the antiferromagnetic component. This implies that the application of an external magnetic field causing the flop transition of the f moments may cause the change in the d-spin structure and accordingly in the electric states.

B. Magnetic-field induced phase transitions

The magnetic-field effect on the temperature dependence of $P_s(\|b)$ is shown in Fig. 5(b). The P_s value was deduced again by measurements of the pyroelectric current in cooling the crystal while applying the electric field (200 kV/m) along the b axis in a constant magnetic field (0–3 T) parallel to the a axis. (The magnetic easy-axis appears to lie within the ab plane.) The critical temperature T_X for the transition between FE3 and X is shifted to lower temperature with the magnetic field, and above 1.5 T the phase X is extinguished and replaced by the FE3 phase. Furthermore, the transition
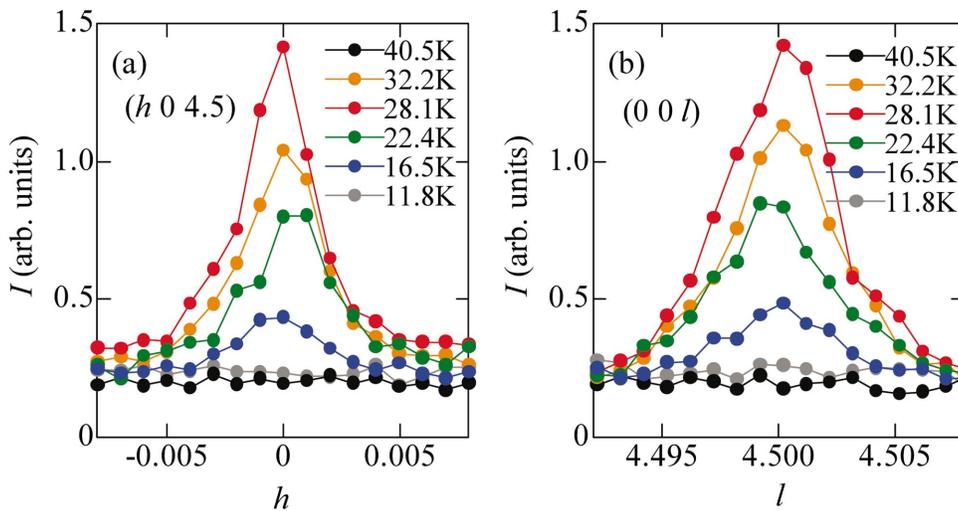
FIG. 4. (Color) X-ray superlattice peak profiles in (a) $(h\ 0\ 4.5)$ and (b) $(0\ 0\ \ell)$ scans at various temperatures in $DyMn_2O_5$.

temperature T_3 between the FE3 and FE2 also shows a shift toward low temperature with increasing magnetic field, and above 2.5 T the FE3 phase also disappears and is transformed into the FE2 phase. Thus, we can present the electric phase diagram in the plane of temperature and magnetic field, as shown in Fig. 5(a). A large field-induced shift is observed for the lower-lying transition temperatures, T_X and T_3, whereas very little for T_2 and T_1. This implies that both the FE3 and the nonpolar phase X are affected by the coupling between the d spins and f moments. Namely, these ferroelectric/paraelectric states at low temperatures are under the influence of f-moment arrangement that is amenable to the external magnetic field.

The magnetic-field induced phase transition as the result of strong coupling between magnetism and ferroelectricity manifests itself also in the isothermal curves of the magnetic-field induced electric-polarization. Figure 6 exemplifies the magnetic-field ($H\|a$) scan at 3 K. Figure 6(b) shows the polarization change derived by the integration of the pyroelectric current while the electric field (200 kV/m) was always applied along the b axis. In the case of zero applied electric field, the direction of the induced polarization was observed not to be uniquely nor controllably fixed, which should be attributed to zero spontaneous polarization in the starting phase X. The magnetic-field-induced polarization appears in a two-step manner as indicated by vertical dashed
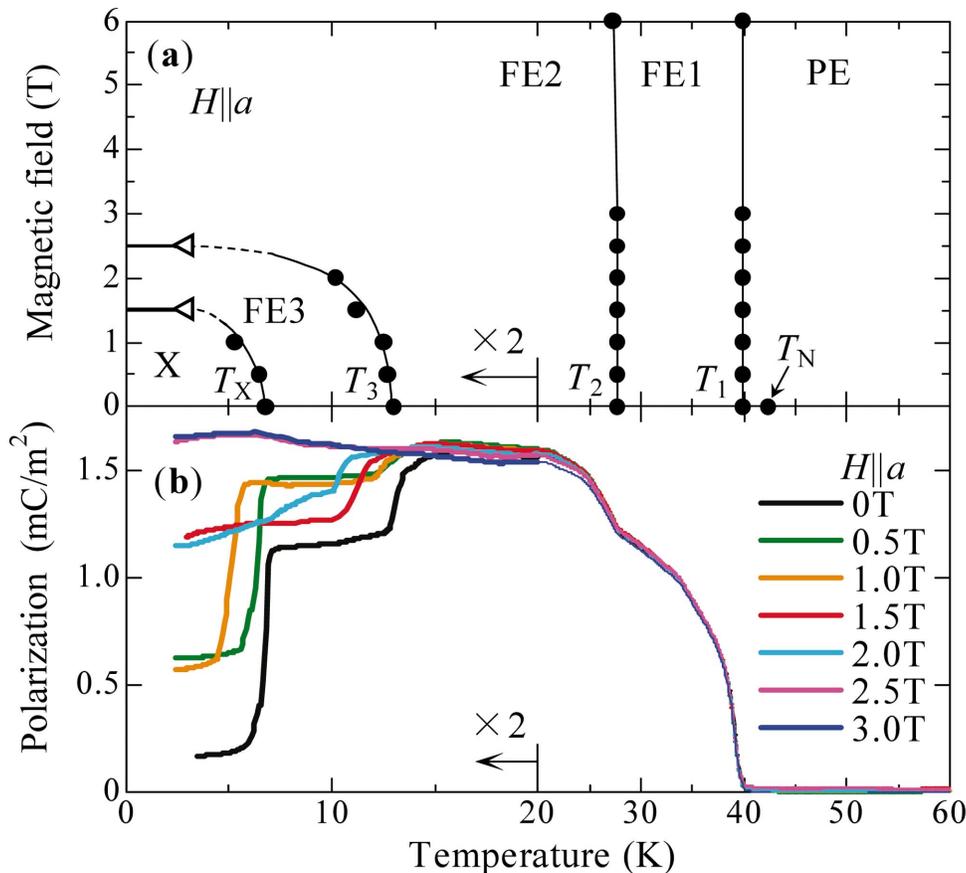

FIG. 5. (Color) (a) The electric phase diagrams (X and PE: paraelectric; FE1, FE2, FE3: ferroelectric) in the plane of temperature and magnetic field as obtained from the measurement on (b) the temperature profile of the polarization ($\|b$) at various magnetic fields. The polarization was deduced by the integration of the pyroelectric current in the electric-field (200 kV/m) cooling run. The electric polarization and the applied magnetic field are parallel to the b and a axis, respectively. Open triangle with horizontal bars in (a) means that the transition does not appear above 3 K.
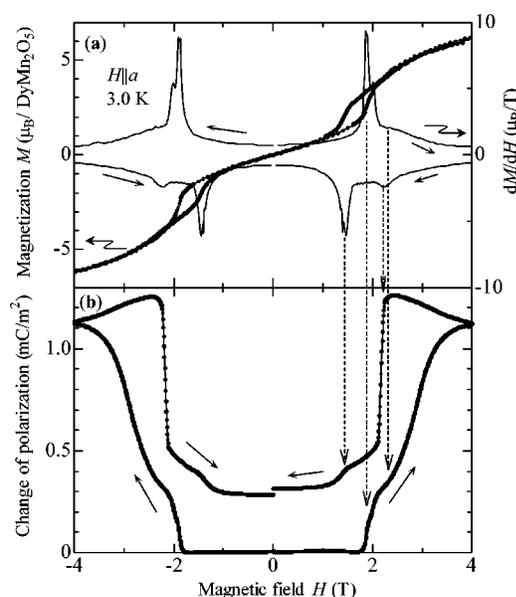
FIG. 6. (a) Magnetization (***M-H***) curves and (b) magnetoelectric effect (***P-H*** curves) in $DyMn_2O_5$ at 3 K. The applied magnetic field ***H*** was parallel to the *a* axis. The magnetization curve shows a clear hysteresis loop around 1.5 T, corresponding to the metamagnetic transition of the Dy *f* moment. The two metamagnetic anomalies are discerned in the ***H*** derivative of magnetization curves as shown by vertical dashed lines in (a) on the ***H***-increasing and -decreasing runs, respectively. (The sign of dM/dH in an ***H***-decreasing run is inverted.) The magnetic field dependence of the electric polarization shown in (b) was measured in an applied electric field of 200 kV/m. In accord with the magnetic transitions, the electric polarization shows the step-like increases (decreases) with increasing (decreasing) ***H***. A large ***H***-hysteretic behavior is also seen in the ***P-H*** curves (b), corresponding to that of the ***M-H*** curve shown in (a), as guided by the vertical dashed lines.

lines. These steps correspond to the transitions to FE3 and FE2, respectively, as noticed from the phase diagram shown in Fig. 5(a). In the ***H*** decreasing run, the two-step anomalies are also observed but respectively accompany the large hysteresis in the transition magnetic field. After the completion of the ***H*** increasing and decreasing run, the total displacement (pyroelectric) current cannot completely cancel out, producing some seemingly finite ***P*** value at the zero magnetic field. This might be due to some residual FE3 phase arising from the strong first-order nature of the transition, and/or due to some leak current because of the procedure of the electric-field application. It is to be noted here that the sign of the ***P*** in the magnetic-field-induced ferroelectric states remains unchanged with the reversal of ***H*** direction, as

far as the small electric field is applied along the same direction during the ***H*** scans. Corresponding to these transition magnetic fields, the magnetization (***M-H***) curves [Fig. 6(a)] show the metamagnetic anomalies corresponding to the flop of the Dy *f* moments. The first one associated with the clear hysteresis loop corresponds to the X-FE3 transition. The anomaly corresponding to FE3-FE2 transition is not so clear in the bare ***M-H*** curve but discernible in its derivative (dM/dH-***H***) curve. Those hysteretic behaviors are also in accord with those of the ***P-H*** curves shown in Fig. 6(b), as guided by the vertical dashed lines. This confirms again that the induced electric polarization arises from the phase transitions mediated by the Zeeman energy but not from the conventional linear ME effect in which the sign reversal should occur upon the reversal of the ***H*** direction.

IV. SUMMARY

The three distinct ferroelectric phases (FE1,2,3) and the lowest-lying reentrant paraelectric phase (X) have been identified in $DyMn_2O_5$. All the ferroelectric phases emerge in the spin-ordered phase perhaps with the commensurate propagation vectors. The coupling between the magnetism and the lattice distortion as the source of the ferroelectricity is also evidenced by the presence of the superlattice peak with twice the magnetic propagation vector in FE1 and FE2 phases. Furthermore, the lower-lying FE3 and paraelectric X phases can be altered by application of external magnetic fields, indicating that these low-temperature dielectric properties are affected also by the Dy *f*-moment order coupled with the Mn *d* spin. In particular, the paraelectric ground state (X) shows the successive ferroelectric transitions to FE3 and then to FE2 with increasing the magnetic field. The magnetic-field induced ferroelectric polarization of about 1 mC/m² is viewed as the gigantic magneto-electric effect. The similar magnetic-field control of the dielectric phase should be ubiquitous in various rare earth (*R*) manganese oxides including families of RMn_2O_5 and $RMnO_3$, in which the Mn *d* electron spins with the large exchange-striction effect as the source of ferroelectricity coupled with the magnetic-field controllable *f* moments of *R* ions.

[1] P. Curie, J. Phys. (Paris), Colloq. **3** (Ser. III), 393 (1894).

[2] I. E. Dzyaloshinskiǐ, Sov. Phys. JETP **10**, 628 (1960).

[3] D. N. Astrov, Sov. Phys. JETP **11**, 708 (1960).

[4] G. T. Rado, Phys. Rev. Lett. **13**, 335 (1964).

[5] E. Fischer, G. Gorodetsky, and R. M. Hornreich, Solid State Commun. **10**, 1127 (1972).

[6] L. M. Holmes, L. G. van Uitert, and G. W. Hull, Solid State Commun. **9**, 1373 (1971).

[7] E. Ascher, H. Rieder, H. Schmid, and H. Stössel, J. Appl. Phys. **37**, 1404 (1966).

[8] T. Kimura, T. Goto, H. Shintani, K. Ishizaka, T. Arima, and Y. Tokura, Nature (London) **426**, 55 (2003).

[9] T. Goto, T. Kimura, G. Lawes, A. P. Ramirez, and Y. Tokura, Phys. Rev. Lett. **92**, 257201 (2004).

[10] I. Kagomiya, K. Kohn, and T. Uchiyama, Ferroelectrics **280**, 297 (2002).

[11] J. A. Alonso, M. T. Casais, M. J. Martínez-Lope, and I. Rasines, J. Solid State Chem. **129**, 105 (1997).

[12] S. C. Abrahams and J. L. Bernstein, J. Chem. Phys. **46**, 3776 (1967).

[13] S. Matsumoto, M. Tanaka, I. Kagomiya, K. Kohn, and S. Naka-mura, Ferroelectrics **286**, 907 (2003).

[14] C. Wilkinson, F. Sinclair, P. Gardner, J. Forsyth, and B. Wanklyn, J. Phys. C **14**, 1671 (1981).

[15] B. Wanklyn, J. Mater. Sci. **7**, 813 (1972).

[16] S. Sawada, Y. Shiroishi, A. Yamamoto, M. Takashige, and M. Matsuo, J. Phys. Soc. Jpn. **43**, 2099 (1977).

[17] K. Aiki, K. Hukuda, H. Koga, and T. Kobayashi, J. Phys. Soc. Jpn. **28**, 389 (1970).